

Interface magnetism in $\text{Fe}_2\text{O}_3/\text{FeTiO}_3$ -heterostructures

Rossitza Pentcheva* and Hasan Sadat Nabi

Department of Earth and Environmental Sciences,
University of Munich, Theresienstr. 41, 80333 Munich, Germany

(Dated: October 22, 2018)

To resolve the microscopic origin of magnetism in the $\text{Fe}_2\text{O}_3/\text{FeTiO}_3$ -system, we have performed density functional theory calculations taking into account on-site Coulomb repulsion. By varying systematically the concentration, distribution and charge state of Ti in a hematite host, we compile a phase diagram of the stability with respect to the end members and find a clear preference to form layered arrangements as opposed to solid solutions. The charge mismatch at the interface is accommodated through Ti^{4+} and a disproportionation in the Fe contact layer into Fe^{2+} , Fe^{3+} , leading to uncompensated moments in the contact layer and giving first theoretical evidence for the *lamellar magnetism hypothesis*. This interface magnetism is associated with impurity levels in the band gap showing halfmetallic behavior and making $\text{Fe}_2\text{O}_3/\text{FeTiO}_3$ heterostructures prospective materials for spintronics applications.

A challenge of today's materials science is to design ferromagnetic semiconductors operating at room-temperature (RT) for spintronics devices. Most of the efforts concentrate on homogeneous doping of semiconductors with magnetic impurities [1, 2, 3, 4], but the interfaces in complex oxides prove to be another source of novel behavior [5, 6, 7]. The unique magnetic properties of the hematite-ilmenite system [8, 9, 10] (a canted antiferromagnet and a RT paramagnet, respectively) currently receive revived interest as a possible cause of magnetic anomalies in the Earth's deep crust and on other planets [11] as well as for future device applications [3, 12, 13].

Both hematite ($a = 5.035\text{\AA}$, $c = 13.751\text{\AA}$ [14]) and ilmenite ($a = 5.177\text{\AA}$, $c = 14.265\text{\AA}$ [15]) crystallize in a corundum(-derived) structure shown in Fig. 1 where the oxygen ions form a distorted hexagonal close packed lattice and the cations occupy 2/3 of the octahedral sites. In $\alpha\text{-Fe}_2\text{O}_3$ (space group $R\bar{3}c$) there is a natural modulation of electronic density along the [0001]-direction where negatively charged 3O^{2-} layers alternate with positively charged 2Fe^{3+} layers. At RT the magnetic moments of subsequent iron layers couple antiferromagnetically (AFM) in-plane with a small spin-canting, attributed to spin-orbit coupling [16, 17, 18]. In ilmenite, FeTiO_3 , Fe- and Ti-layers alternate, reducing the symmetry to $R\bar{3}$ and the corresponding sequence is $3\text{O}^{2-}/2\text{Fe}^{2+}/3\text{O}^{2-}/2\text{Ti}^{4+}$ with AFM coupling between the Fe layers and $T_N = 56\text{-}59\text{ K}$ [19].

At the interfaces (IFs) in hematite-ilmenite ex-solutions, charge neutrality is disrupted. One way to balance the excess charge at the interface is by a disproportionation in the Fe layer, now becom-

ing mixed Fe^{2+} and Fe^{3+} . This *lamellar magnetism hypothesis (LMH)* was proposed by Robinson *et al.* [20] based on bond valence models and kinetic Monte Carlo simulations (kMC) with empirical chemical and magnetic interaction parameters. The increased technological interest in this system calls for an atomistic material specific understanding that can only be obtained from first principles calculations. A previous density functional theory (DFT) study within the generalized gradient approximation (GGA) found no evidence for the LMH [21]. However, electronic correlations, not included in the local (spin-) density approximation (LSDA) or GGA of DFT, play an important role in transition metal oxides. Such effects were considered recently within LSDA+U [22] or using hybrid functionals [23] for

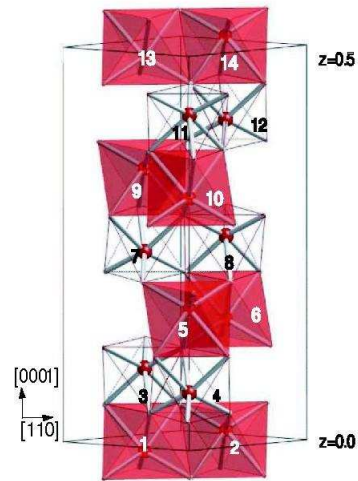


FIG. 1: (Color online) Crystal structure of FeTiO_3 , showing half of the 60 atom unit cell. The cation sites are numbered, oxygen occupies the edges of the octahedra.

*Electronic address: pentcheva@lrz.uni-muenchen.de

single Ti impurities in hematite, however layered arrangements and interfaces were not addressed.

In this paper we have performed DFT calculations including a Hubbard U [24] for the end members Fe_2O_3 and FeTiO_3 , as well as their interfaces and solid solutions (SS). By varying systematically the concentration, distribution and charge state of Ti incorporated in a α - Fe_2O_3 -host, we explore different scenarios for the charge compensation mechanism and its consequences for the magnetic and electronic behavior. Finally, we compile a phase diagram of the stability of the different configurations with respect to the end members as a function of Ti-doping also taking into account the effect of strain.

Our DFT-GGA [26] calculations are performed using the all-electron full-potential augmented plane waves (FP-APW) method as implemented in WIEN2k [25]. Electronic correlations are considered within the fully localized limit (LDA+ U) [24]. The systems are modeled in the hexagonal primitive unit cell (shown in Fig. 1) containing 30 and 60 atoms. For these 24 and 15 k -points in the irreducible part of the Brillouin zone were used, respectively. Inside the muffin tins ($R_{\text{MT}}^{\text{Fe,Ti}} = 1.80$ bohr, $R_{\text{MT}}^{\text{O}} = 1.60$ bohr) wave functions are expanded in spherical harmonics up to $l_{\text{max}}^{\text{wf}} = 10$ and non-spherical contributions to the electron density and potential up to $l_{\text{max}}^{\text{pot.}} = 6$ are used. The energy cutoff for the plane wave representation in the interstitial is $E_{\text{max}}^{\text{wf}} = 19$ Ry for the wave functions and $E_{\text{max}}^{\text{pot.}} = 196$ Ry for the potential. These convergence parameters ensure a numerical accuracy of energy differences better than 0.01eV/60 atom cell. A full structural optimization of internal parameters has been performed [27].

As a starting point we have modeled the end members Fe_2O_3 and FeTiO_3 . In agreement with previous calculations [22, 28], GGA+ U considerably improves the band gap of hematite from 0.43 eV (GGA) to 2.2 eV for $U=6$ eV and $J=1$ eV in close agreement with measured values of 2.14-2.36 eV [29, 30]. Also the type of band gap changes from a Mott-Hubbard between $\text{Fe}3d$ - $\text{Fe}3d$ states to charge transfer after the scheme of Zaanen *et al.* [31] between occupied $\text{O}2p$ and empty $\text{Fe}3d$ -states.

For ilmenite GGA incorrectly predicts a metallic state [32], hence the inclusion of Hubbard U ($U = 8$ eV, $J = 1$ eV) is decisive to obtain a Mott-Hubbard gap of 2.18 eV ($\Delta^{\text{exp}} = 2.54$ eV [9]) between the occupied $\text{Fe}d_{z^2}$ -orbital and the unoccupied $\text{Fe}3d$ states in one spin channel (all $\text{Fe}3d$ orbitals being occupied in the other spin-channel). These U and J values are used both on Fe and Ti in the following. A $\text{Fe}^{3+}/\text{Ti}^{3+}$ charge arrangement lies 0.63 eV/p.f.u. above the ground state $\text{Fe}^{2+}/\text{Ti}^{4+}$. For $\text{Fe}^{2+}\text{Ti}^{4+}\text{O}_3$ the AFM and FM coupling between Fe-layers is nearly degenerate, consistent with the

TABLE I: Relative stability (eV/60 at. cell) of the different cation arrangements in the Ti^{4+} , Fe^{2+} , Fe^{3+} charge state (strained at the Fe_2O_3 lattice parameters) with respect to the most stable configuration whose energy is set to 0.0 eV. The positions occupied by Ti are denoted as subscripts according to Fig. 1 (SSL: spin-sublattice). The total magnetic moment, electronic behavior (hm/m denotes halfmetallic/metallic) as well as Ti^{4+} -O and Fe^{2+} -O distances at the interface are also displayed.

System	ΔE (eV)	$d_{\text{Ti}^{4+}-\text{O}}$ Å	$d_{\text{Fe}^{2+}-\text{O}}$ Å	M_{tot} (μ_B)	Δ (eV)
Ilm ₁₇					
T _{1,2} : 1 Ti-layer	0.0	1.90	2.08	-8.0	hm
T ₇ : single impurity	0.20	1.93	2.02	12.0	hm
Ilm ₃₃					
T _{1,2,13,14} : 1 Ti-layer	0.36	1.90	2.08	-16.0	hm
T _{3,4} : 2 Ti-layers	0.00	1.89	2.08	16.0	hm
T _{5,10} : same SSL	0.19	1.86	2.04	-16.0	hm
T _{5,7} : different SSL	0.41			0.0	m
T _{5,8} : different SSL	1.24	1.86	2.06	0.0	hm
Ilm ₅₀					
T _{1,2,5,6} : 3 Ti-layers	0.00	1.90	2.07	-24.0	hm
T _{3,4,7} : Ti-Fe@IF	1.23	1.96	2.00	8.0	hm
Ilm ₆₆					
T _{3,4,11,12} : 4 Ti-layers	0.00	1.90	2.07	16.0	hm
T _{3,6,9,12} : SS	0.95	1.92	2.02	0.0	hm

low T_N .

In the following we vary the concentration and distribution of Ti in a Fe_2O_3 -host. The positions of the Ti-ions are given as subscripts and follow the notation of Fig. 1, e.g. T_{3,4,7,8,11,12} describes pure ilmenite. Table I contains the energetic stability, structural, magnetic and electronic properties of different cation arrangements and concentrations. We start the discussion with Ilm₃₃ which corresponds to four Ti-ions out of 24 cations in the 60-atom cell. We find that the formation of a compact ilmenite-like block with a Fe-layer sandwiched between two Ti-layers (T_{3,4}), is by 0.36 eV more favorable than incorporation of single Ti layers in the hematite host (T_{1,2,13,14}). The spin density of T_{3,4} plotted in Fig. 2a) shows that the central Fe-layer turns into Fe^{2+} and the charge mismatch at the IF is compensated by $\text{Fe}^{2+}, \text{Fe}^{3+}$ in the contact layer, giving theoretical evidence from first principles for the *lamellar magnetism* hypothesis of Robinson *et al.* [20]. Our GGA+ U calculations show that Ti^{4+}_4 shares faces with Fe^{3+}_5 , while Fe^{2+}_6 shares faces with Fe^{3+}_8 from the next hematite layer. Such a configuration was proposed using bond-valence sums [33] and kMC [34] only after considering both chemical and magnetic interactions.

The formation of layered arrangements (T_{3,4}) is favored compared to a more random distributions with 50% substituted cation layers (e.g. T_{5,10}, T_{5,7}

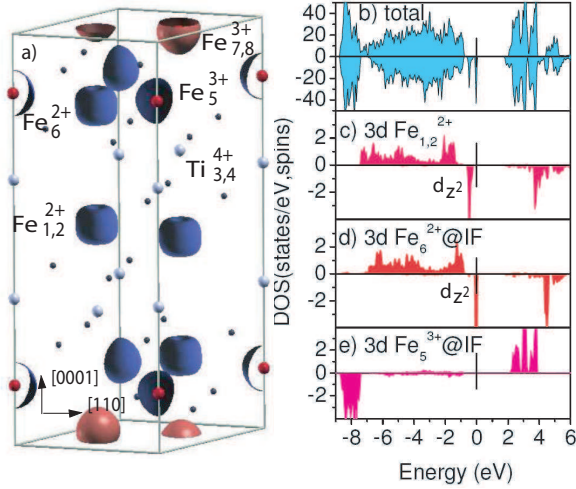


FIG. 2: (Color online) a) Spin density distribution and b-e) total and projected density of states of Ti double layer in hematite ($T_{3,4}$) with $Fe^{2+}_{1,2}$, $Ti^{4+}_{3,4}$ and a disproportionated Fe^{3+}_5 , Fe^{2+}_6 layer at the interface. The position of the Fermi level is set to 0.0 eV and denoted by a short line. In a) positions of Ti, Fe and O are marked by light grey, red and small black circles, respectively.

or $T_{5,8}$). With respect to magnetism, each Ti ion adds a magnetic moment of $4\mu_B$ independent of whether the extra electron is localized at Ti (Ti^{3+}) or at a neighboring Fe (Fe^{2+}). In solid solutions the total magnetic moment depends on the site and sublattice where Ti is built in. We find that incorporation in the same spin-sublattice $T_{5,10}$ (which maximizes the magnetic moment) is favored by 0.22 eV compared to the AFM $T_{5,7}$. Taking into account local lattice relaxations enhances the energy gain compared to previous calculations by Velez *et al.* (0.08 eV)[22]. Still, some degree of Ti disorder is likely in quickly cooled samples, reducing the expected magnetization as observed by Chambers *et al.* [3] ($0.5 \pm 0.15 \mu_B/Ti$ for $x_{Ti} = 0.15$). For higher Ti concentrations and longer annealing steps the formation of the thermodynamically more stable layered ferrimagnetic phase is expected, consistent with the strong correlation between cation order and ferrimagnetism found in annealed samples [8, 12] and the saturation magnetization of $3\mu_B/mol$ measured in epitaxial films with $x_{Ti} \leq 0.63$ [13]. While below the ordering temperature of ilmenite only ilmenite lamella with an odd number of Ti-layers are expected to carry a non-zero magnetization, above 56 K the net magnetic moment will be solely due to the uncompensated magnetic moments in the contact layers, independent of the number of Ti-layers within the paramagnetic ilmenite lamella.

Concerning the electronic properties, doping Fe_2O_3 with Ti leads to impurity levels in the

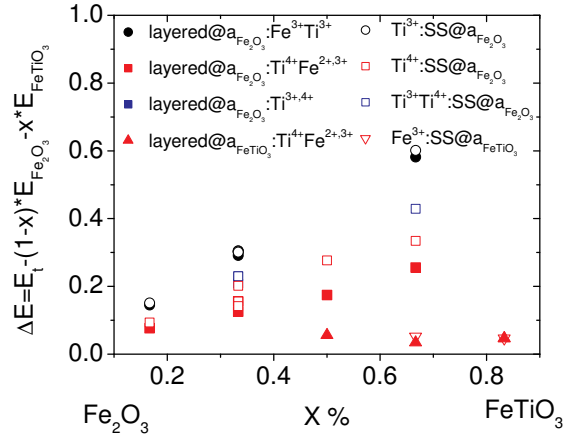


FIG. 3: (Color online) Formation energy (eV/p.f.u.) with respect to the end members as a function of ilmenite concentration x . Layered arrangements (solid solutions) are denoted by full (open) symbols.

band gap arising from the occupied d_{z^2} -orbital of Fe^{2+} ions in the contact layer. The density of states plotted in Fig. 2b-e) shows that these states are pinned at the Fermi level, leading to fully spin-polarized carriers and half-metallic behavior for $T_{3,4}$. This trend is robust with respect to U [35] and is observed for most of the studied cation concentrations and arrangements after structural relaxation. Experimentally, semiconducting behavior and a drop in resistivity of several orders w.r.t. the end members is measured [3, 9, 12, 13] with values suggesting localized rather than itinerant carriers consistent with the picture we obtain from LDA+U.

Next we turn to the energetic stability as a function of the Ti-concentration displayed in Table I and the phase diagram in Fig. 3. Charge compensation through Ti^{4+} and disproportionation of iron into Fe^{2+} , Fe^{3+} is strongly favored compared to compensation involving Ti^{3+} , especially after optimization of the internal structural parameters. Moreover, the formation of layered configurations (full symbols) is preferred over disordered arrangements (empty symbols) except for very high ($> 83\%$) and very low concentrations ($< 17\%$), consistent the miscibility gap from thermodynamic data (e.g. [21, 36]). The linear increase of formation energy in the range between Ilm_{17} and Ilm_{66} indicates that straining Ti doped Fe_2O_3 to the Fe_2O_3 lattice parameters gets increasingly unfavorable with growing x . On the other hand, using the ilmenite lattice parameters at $x = 66\%$ instead of hematite (volume increase of 8.7%) leads to an energy gain of 0.22 eV/p.f.u. for $T_{7,8,11,12}$ (red filled up-triangles in Fig. 3).

An interesting trend is observed in the shortest cation-oxygen bond lengths (cf. Table I), which

tend to relax towards the values in the respective end member. While $d_{\text{Fe}^{3+}-\text{O}}$ (not shown) remains close to the value in bulk hematite (1.96Å), the bond lengths of the Ti-impurity and the neighboring Fe^{2+} relax towards the values in bulk ilmenite (1.92 and 2.07Å, respectively).

In Fe doped ilmenite the trend towards layered arrangements is retained for 66%, e.g. $\text{T}_{7,8,11,12}$ is favored by 0.21 eV compared to $\text{T}_{3,8,11,12}$, but ordered and disordered phases are nearly degenerate at 83%. Fe substituting for Ti in the ilmenite lattice is Fe^{3+} . Additionally, one Fe in the neighboring layer turns Fe^{3+} to compensate the charge, forming a Fe^{2+} , Fe^{3+} contact layer. The substituted Fe shows a very strong tendency to couple antiparallel to the neighboring Fe-layers.

In summary, we present a comprehensive GGA+U-study of the cation, charge and magnetic order in the hematite-ilmenite system showing a strong preference towards formation of layered configurations as opposed to solid solutions. At the interface between hematite and ilmenite blocks we find evidence for the *lamellar magnetism hypothesis* [20] with a disproportionated Fe^{2+} , Fe^{3+} contact

layer to accommodate the polar discontinuity. These uncompensated moments lead to ferrimagnetic behavior of the system. The d_{z^2} orbital in one spin-channel (all d orbitals being occupied in the other) at the Fe^{2+} -sites in the contact layer crosses the Fermi level leading to halfmetallic behavior in most of the studied compositions. The ferrimagnetism emerging at the interface of two antiferromagnetic oxides like hematite and ilmenite is an impressive example of the novel functionality that can arise as a consequence of a polar discontinuity and the richer possibilities to compensate it that complex oxides offer. Recently, an exchange bias of more than 1 Tesla was reported in this system [37]. Further phenomena such as oscillatory exchange coupling and spin-polarized transport remain to be explored in controlled epitaxial Fe_2O_3 - FeTiO_3 -multilayers on the route to possible device applications.

We acknowledge gratefully discussions with M. Winklhofer, W. Moritz and R. Harrison as well as funding by the DFG (Pe883/4-1) and ESF within the European Mineral Science Initiative (EuroMinSci). Simulations are performed on the high performance supercomputer at the Leibniz Rechenzentrum.

-
- [1] J. M. D. Coey, M. Venkatesan, and C. B. Fitzgerald, *Nature Mater.* **4**, 173 (2005).
 - [2] A. H. MacDonald, P. Schiffer and N. Samarth, *Nature Mater.* **4**, 195 (2005).
 - [3] S. A. Chambers *et al.*, *Materials Today* **9**, 28 (2006).
 - [4] S. Kuroda *et al.*, *Nature Mater.* **6**, 440 (2007).
 - [5] A. Ohtomo *et al.*, *Nature* **419**, 378 (2002).
 - [6] A. Brinkman *et al.*, *Nature Mater.* **6**, 493 (2007).
 - [7] N. Reyren *et al.*, *Science* **317**, 1196 (2007).
 - [8] Y. Ishikawa and S. Akimoto, *J. Phys. Soc. Jpn.* **12**, 1083 (1957).
 - [9] Y. Ishikawa, *J. Phys. Soc. Jpn.* **13**, 37 (1958).
 - [10] C. M. Carmichael, *Proc. R. Soc. London A* **263**, 508 (1961).
 - [11] T. Kasama *et al.*, *Earth Planet. Sci. Lett.* **224**, 461 (2004).
 - [12] Y. Takada *et al.*, *J. Magn. Magn. Matter.* **310**, 2108 (2007).
 - [13] H. Hojo *et al.*, *Appl. Phys. Lett.* **89**, 142503 (2006).
 - [14] D. A. Perkins and J. P. Attfield, *J. Chem. Soc., Chem. Commun.*, 229 (1991).
 - [15] R. J. Harrison, S. A. T. Redfern, and R. I. Smith, *Am. Miner.* **85**, 194 (2000).
 - [16] L. M. Sandratski and J. Kübler, *Europhys. Lett.* **33**, 447 (1996).
 - [17] I. J. Dzialoshinski, *Phys. Chem. Solids* **4**, 241 (1958).
 - [18] T. Moriya, *Phys. Rev.* **120**, 91 (1960).
 - [19] P. F. McDonald *et al.*, *J. Appl. Phys.* **69**, 1104 (1991).
 - [20] P. Robinson *et al.*, *Nature* **418**, 517 (2002).
 - [21] B. P. Burton, A. Chaka, and D. J. Singh, *Phase Trans.* **78**, 239 (2005).
 - [22] J. Velev *et al.*, *Phys. Rev. B* **71**, 205208 (2005).
 - [23] T. Droubay *et al.*, *Phys. Rev. B* **75**, 104412 (2007).
 - [24] V. I. Anisimov *et al.*, *Phys. Rev. B* **48**, 16929 (1993).
 - [25] P. Blaha, *et al.*, (Karlheinz Schwarz, Techn. Universität Wien, Austria), 2001, ISBN 3-9501031-1-2.
 - [26] J. P. Perdew, K. Burke, and M. Ernzerhof, *Phys. Rev. Lett.* **77**, 3865, (1996).
 - [27] F. Tran *et al.*, *Comput. Phys. Commun.*, submitted.
 - [28] G. Rollmann *et al.*, *Phys. Rev. B* **69**, 165107 (2004).
 - [29] D. Benjelloun *et al.*, *Mater. Chem Phys.* **10**, 503 (1984).
 - [30] R. H. Chang and J. B. Wagner, *J. Am. Cer. Soc.* **55**, 211 (1972).
 - [31] J. Zaanen, G. A. Sawatzky, and J. W. Allen, *Phys. Rev. Lett.* **55**, 418 (1985).
 - [32] N. C. Wilson *et al.*, *Phys. Rev. B* **71**, 075202 (2005).
 - [33] P. Robinson, R. J. Harrison, and S. A. McEnroe, *Am. Miner.* **91**, 67 (2006).
 - [34] R. J. Harrison, *Am. Miner.* **91**, 1006 (2006).
 - [35] The same halfmetallic behavior is obtained also for a lower U value of 6 eV.
 - [36] S. A. McEnroe *et al.*, *Geophys. J. Int.* **151** 890 (2002).
 - [37] S. A. McEnroe *et al.*, *Nature Nanotechn.* **2**, 631(2007).